

# JoIN: Joint GANs Inversion for Intrinsic Image Decomposition

Viraj Shah\*  
UIUC

vjshah3@illinois.edu

Svetlana Lazebnik  
UIUC

slazebni@illinois.edu

Julien Philip  
Adobe Research

juphilip@adobe.com

## Abstract

*In this work, we propose to solve ill-posed inverse imaging problems using a bank of Generative Adversarial Networks (GAN) as a prior and apply our method to the case of Intrinsic Image Decomposition for faces and materials. Our method builds on the demonstrated success of GANs to capture complex image distributions. At the core of our approach is the idea that the latent space of a GAN is a well-suited optimization domain to solve inverse problems. Given an input image, we propose to jointly invert the latent codes of a set of GANs and combine their outputs to reproduce the input. Contrary to most GAN inversion methods which are limited to inverting only a single GAN, we demonstrate that it is possible to maintain distribution priors while inverting several GANs jointly. We show that our approach is modular, allowing various forward imaging models, and that it can successfully decompose both synthetic and real images.*

## 1. Introduction

Any natural image can be seen as an intricate combination of geometry-dependent, material-dependent, and lighting-dependent components. Decomposing an image in such components, a problem known as intrinsic image decomposition (IID) allows for varying each property independently in order to achieve complex image editing [13].

While the forward mapping from the decomposed image components to the natural image is direct, the inverse process is a challenging ill-posed problem. To obtain a useful decomposition it is usual to constrain the solution space by employing either hand-crafted [5, 69] or learned priors [47]. However, these priors are often restricting the solution too much or lead to cross-contamination where texture is copied in shading and albedo exhibits shading variations.

Recently, there has been a growing interest in employing Generative Adversarial Networks (GANs) as priors in a variety of inverse imaging problems such as image inpainting [12, 27, 78], HDR imaging [56], image super-

resolution [12, 27, 44], compressive sensing [12, 66], and phase retrieval [29, 33], owing to their tremendous success in mimicking real data distributions. A common way to leverage these GAN priors is to invert the mapping of the GAN – a highly challenging problem known as GAN Inversion. While existing GAN Inversion methods are limited to inverting only a single GAN, in this work we propose to jointly invert multiple GANs to decompose natural image. Contrary to previous work in which all components are known in advance and have to be generated by the same GAN [28], we propose to train multiple GANs independently. We show this prevents channel cross-contamination and also allows flexible forward and inverse models as the number of components and the way they are combined does not have to be pre-determined.

We apply this new approach to intrinsic image decomposition by training a bank of GANs for components such as albedo or shading. During inversion, to ensure that each intrinsic component remains on the distribution manifold of its associated GAN we propose a new kNN-based loss regularization to constrain the optimization. We further demonstrate that both encoder-based GAN initialization and generator tuning techniques from the existing literature can be used on this joint inversion problem, improving the results. We test and evaluate our method on two types of datasets, faces and materials. To summarize, we introduce a novel framework to solve image-based inverse problems which we apply to IID with the following key contributions:

- We propose to use a bank of GANs as a prior to solve inverse problems by jointly inverting them.
- We introduce a novel kNN-based regularization term for GAN inversion allowing them to better retain their distribution properties than existing in-domain loss.
- We show that this approach is both flexible and compatible with existing GAN inversion techniques.

## 2. Related Work

### 2.1. Image Decomposition

The intrinsic decomposition of images is a long-standing problem that emerged with the retinex and lightness theory

\*Work done during an internship at Adobe Research

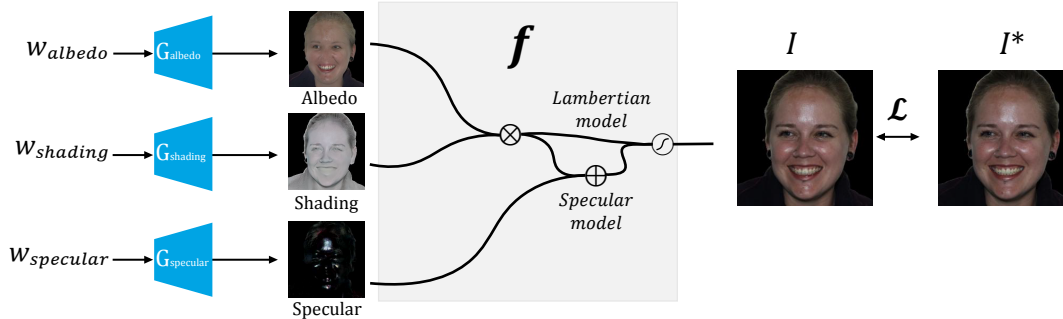


Figure 1. **Overview of our approach.** We train multiple GANs, each trained only on a single image component, their output is combined using a function  $f$ . The latent codes of each GAN are optimized to minimize the loss between the target image  $I^*$  and the output  $I$ .

[30, 42]. Using a purely diffuse model, early work computed shadow-free reflectance images of faces [74] using time-lapse sequences. User-assisted methods were the first to successfully tackle the problem for single natural images [13, 70]. With the rise of deep learning a large body of work emerged using neural networks to predict intrinsic images [45–47, 55, 80, 83]. Recently, Liu et al. [50] presented a method, sharing some ideas with our pipeline. They build priors independently for shading and reflectance using image collections and adversarial auto-encoders. Contrary to our approach, they use a fixed forward model and would require full retraining if a component such as specular were to be added.

For photo collections, many works explored this problem using geometry priors [24, 40, 41, 59, 60], and recently methods were introduced working on videos [11, 52, 53, 77]. One of the main applications of IID lies in image relighting for which decomposing an image in specific components such as albedo, shading, shadows or normals is often an intermediate step both for faces [31, 57, 79] and outdoor picture [26]. In the context of the more constrained problem of material acquisition, methods often aim at recovering richer information. They usually predict a full SVBRDF map composed of albedo but also normals, roughness, and specular maps [3, 19, 20]. Some recent methods proposed to use adversarial networks as part of their SVBRDF estimation pipelines [84, 85]. Closer in spirit to our method MaterialGAN [28] proposes to use a single GAN trained on all the channels of SVBRDF maps and to invert a latent code to recover an SVBRDF. Contrary to our method it requires several input images and known lighting conditions for each input.

## 2.2. GAN Priors and GAN Inversion

Inverting a GAN to obtain the latent code corresponding to an image is a key step in solving inverse problems [67]. Owing to its importance, many GAN inversion approaches have been recently proposed as reviewed in [75]. We can classify these methods in three broad classes: optimization-

based, encoder-based, and hybrid.

**Optimization-based methods** such as [1, 2, 17, 38, 48, 49, 86] regress a latent code using gradient descent by minimizing a loss between a target image and the generated image produced by the latent code. The key variations among these approaches are the latent space chosen for the optimization ( $\mathcal{Z}$  space,  $\mathcal{W}$  space,  $\mathcal{W}^+$  space, etc.); the loss function(s) they use to calculate the similarity between the target and the estimate; and additional criterion used for aiding optimization (such as regularization, improved initialization, and early stopping). Although these methods can produce relatively precise outcomes, their iterative optimization scheme is slower than forward methods and can converge to local minima when badly initialized.

Contrary to optimization-based approaches, **encoder-based methods** propose to use an end-to-end framework based in which an encoder that takes the target image as input, predicts the latent code directly [4, 14, 15, 43, 51, 54, 58, 61, 63, 71–73, 75, 76, 86]. These different methods propose powerful encoder architectures, specialized loss functions, and training procedures adapted to GAN inversion. The main advantage of encoder-based methods is their faster inference times, but they generally suffer from lower result quality and worse generalization. This makes them great candidates to serve as an initializer for optimization-based inversion. Methods that combine both optimization and encoder-based initialization are typically known as **Hybrid approach** [4, 6–8, 16, 32, 73, 86].

Recently, a fourth category of approaches has emerged that advocates fine-tuning the generator weights after optimizing the latent code [25, 65]. Such methods produce better reconstruction since the generator is allowed to fit the target image but fine-tuning the generator can lead to distortions in the generator manifold losing important properties. While our proposed method and contributions are orthogonal to the different inversion approaches we show that they are compatible with joint GAN inversion. More recently, [9] has shown that StyleGAN has an internal representation of intrinsic images that can be accessed by find-

ing an appropriate offset to the latent codes. However, this method is not applicable for real images, since the offsets obtained are not compatible with the output latent codes of the GAN inversion on the real image.

### 3. Our Approach

In this work, we propose to solve intrinsic image decomposition using an optimization formulation that leverages a bank of GANs as priors. Our aim is to decompose a natural image into its material-dependent and lighting-dependent components such as albedo and shading. This inverse problem is ill-posed, and priors on the structure of each image component are required to obtain a solution.

Each image component distribution can be closely approximated using a GAN model. We propose to create a bank of GANs that consists of one GAN model for each image component that we desire to recover. Since each GAN maps a lower dimensional latent space to an image component space, solving the inverse problem aims to recover the latent codes corresponding to each image component which can be formulated as the joint inversion of multiple GANs.

In this section, we first present our optimization framework and its constraints, then we introduce a novel loss that helps further regularize the optimization and maintain the GANs priors.

#### 3.1. JoIN: Joint Inversion of Multiple GANs

Given an image  $I^*$ , and a forward differentiable function  $f$  taking as input  $n$  image components  $C_{1\dots n}^*$  we suppose that  $I^*$  can be modeled as:

$$I^* = f(C_1^*, \dots, C_n^*) \quad (1)$$

Where we assume  $f$  is known. We aim at recovering  $C_{1\dots n}^*$  given only  $I^*$  as input. Instead of directly optimizing  $C_{1\dots n}^*$  to recover  $C_{1\dots n}^*$  in the image domain we propose to represent them as the output of a GAN  $G_i$  for a latent code  $w_i$ :

$$C_i = T_i^{-1}(G_i(w_i)) \quad (2)$$

Where  $T_i^{-1}$  is an inverse color transform operator.

For  $G_i$  we follow the architecture of StyleGAN2 [37] where  $w_i$  is in the  $\mathcal{W}$  space. Our estimate of  $I$  is thus given by:

$$I(w_1, \dots, w_n) = f(T_1^{-1}(G_1(w_1)), \dots, T_n^{-1}(G_n(w_n))) \quad (3)$$

Our goal is thus to find the  $w_i, i \in 1 \dots n$  that minimize a reconstruction loss function  $\mathcal{L}$ :

$$\arg \min_{w_i, i \in 1 \dots n} \mathcal{L}(I^*, I(w_1, \dots, w_n)). \quad (4)$$

Eq. 4 is analogous to the standard GAN inversion formulation, except for the fact that it aims to invert  $n$  Generators simultaneously instead of one. The loss in Eq. 4 is minimized over all the latent codes  $w_i$ s simultaneously, and the final estimates  $\hat{w}_i$ s can be passed to Eq. 2 to obtain the image components  $C_{1\dots n}^*$ . We use E-LPIPS loss [39] (robust version of LPIPS [82] perceptual loss) as the loss function  $\mathcal{L}$  unless otherwise specified.

#### 3.2. Intrinsic image decomposition

In this paper we focus on the problem of intrinsic image decomposition. We thus adapt the general formulation presented in the previous section.

We first consider a simple forward model assuming Lambertian surfaces. It uses two components – albedo and shading to represent the image:

$$I^* = sRGB(C_{albedo} * C_{shading}). \quad (5)$$

Then we consider a non-Lambertian model with a separate specular component:

$$I^* = sRGB(C_{albedo} * C_{shading} + C_{specular}). \quad (6)$$

#### 3.3. Optimization-based Joint Inversion

Given a forward model described in Eq. 5 or Eq. 6, we first train a GAN for each intrinsic component (albedo, shading and eventually specular images) independently using the StyleGAN2 architecture [36, 38]. As the GANs are trained independently the forward model can be chosen after the fact and components replaced or added, we also demonstrate in Sec. 5.4 that training independent GANs helps prevent channel cross-contamination.

Given the pre-trained GANs and an input  $I^*$ , we then optimize latent codes  $w_i^*$  by minimizing the loss function in Eq. 4 over  $w_i$ s using gradient descent. Note that our optimization is only guided by the input image  $I^*$  since the loss in Eq. 4 is calculated on the combination of all the estimated components.

#### 3.4. kNN loss

Allowing the latent codes  $w_i$  to explore freely the space during optimization can lead to cross-contamination as they deviate from the manifold of possible  $w$  within  $\mathcal{W}$ . In such case the generator for a component  $C_i$  starts producing signals corresponding to another component  $C_j$ . We thus propose a new kNN-based regularization loss to constrain the latent codes to stay within domain.

To this end, we take inspiration from previous works [71, 87], which introduces an in-domain loss on the latent codes as follows:

$$\mathcal{L}_{in} = \|w_i - \bar{w}\|_2, \quad (7)$$

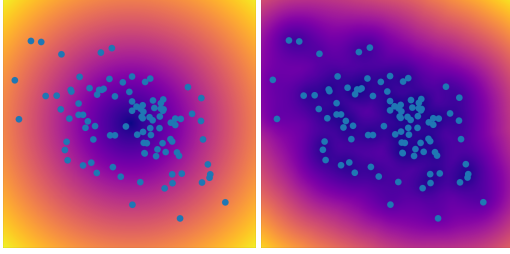


Figure 2. **Loss landscapes for 2D latent vectors.** Dots represent randomly sampled latent vectors and the colormap the intensity of the loss. 100 samples,  $k=5$  NN. Left: using in-domain formulation. Right: using our knn loss. Ours allows to better capture the diversity of the distribution and is lower at boundaries.

where  $\bar{w}$  is the average  $w$  obtained by drawing  $100k$  random samples of random normal code  $z$ . This in-domain loss tries to keep the optimized latent close to the distribution mean in order to keep the estimate within the training domain. We argue that this formulation has two main drawbacks. First, using the distribution mean penalizes the solution space near the boundary of the distribution. Second, it assumes that the distribution of  $w$  is isotropic, which has no reason to hold given the use of a non-linear mapping network during training. As a remedy, we propose a novel  $k$ -Nearest Neighbors-based loss formulation that better allows the exploration of the full domain. We first sample a large number ( $100k$ ) of  $z$  codes from a truncated Gaussian distribution to obtain a set of  $w$  codes  $W$ .

Then, during inversion, at each step, we calculate the  $k$  nearest neighbors of the current latent code estimate  $kNN(w_i)$ , and use a softmax weighted average of the distance to nearest neighbors as a loss:

$$\mathcal{L}_{kNN} = \sum_{w_i^k \in kNN(w_i)} \|w_i - w_i^k\|_2 \cdot \frac{e^{-0.5 \frac{\|w_i - w_i^k\|_2}{\bar{d}_i^k}}}{D_i} \quad (8)$$

where  $D_i$  is the normalizing factor:

$$D_i = \sum_{w_i^k \in kNN(w_i)} e^{-0.5 \frac{\|w_i - w_i^k\|_2}{\bar{d}_i^k}} \quad (9)$$

And  $\bar{d}_i^k$  is the mean distance to nearest neighbors:

$$\bar{d}_i^k = \sum_{w_i^k \in kNN(w_i)} \|w_i - w_i^k\|_2 \quad (10)$$

Figure 2 provides an intuitive visualization of our kNN loss in 2D. Our loss landscape does not penalize as much the exploration of the distribution and its boundaries. We provide the results of our optimization scheme and ablation studies demonstrating the benefits of our loss in Sec. 5.

## 4. Adapting existing inversion methods

In this section we show how existing initialization and generator fine-tuning mechanisms can be adapted to JoIN to improve the inversion result.

### 4.1. Encoder-guided Initialization

While our optimization-based approach produces faithful decompositions on synthetic data, the optimization can get stuck in local minima if the initial latent codes lie far from the target codes. To make our approach more robust, we propose to use an encoder-guided initialization inspired by hybrid approaches of GAN inversion [8, 16, 73]. For each component, we can independently train a pSp network [63] to encode a natural image into a latent code  $w$  used by the pre-trained generator to recover the given component. At test time, given a natural image, the latent code produced by the encoder can be used as an initialization for the optimization.

### 4.2. Generator fine-tuning - PTI

Recently, approaches using generator fine-tuning have emerged [25, 65]. First, a  $w$ -code is estimated using an off-the-shelf inversion technique, and then with the fixed  $w$  pivot, the generator is updated to obtain close to zero reconstruction errors.

In our case, the generator fine-tuning scheme can be defined as:

$$\arg \min_{\theta_{G_i}, i \in 1 \dots n} \mathcal{L}(I^*, f(T_1^{-1}(G_1(\widehat{w}_1)), \dots, T_n^{-1}(G_n(\widehat{w}_n)))) \quad (11)$$

where  $\theta_{G_i}$  represents trainable parameters of the generator  $G_i$  that corresponds to the component  $C_i$ , and  $\widehat{w}_i$ s are output of the optimization.

While direct fine-tuning allows the generator to overfit to the target image perfectly, it distorts the GAN manifold. In our case, allowing multiple GANs to fine-tune at once can result in loss of the priors and cross-contamination (see Fig. 13 *w/o D Loss*). Therefore, we rely on the discriminator loss to regularize the fine-tuning [25]. While fine-tuning the generator around the  $\widehat{w}_i$  pivot, we apply a new localized discriminator loss  $\mathcal{L}_{LD}$ , we refer to it as *D Loss*.

Specifically, we sample  $n_a$  number of anchor latent codes in the close vicinity of our fixed  $w$ -code by interpolating  $\widehat{w}_i$  with randomly sampled codes  $w_k$ . At each fine-tuning step, we pass the anchor codes through the generator and compute the discriminator loss on the resulting images, keeping the discriminator frozen:

$$\mathcal{L}_{LD} = \sum_i \sum_{k=1}^{n_a} D_i(G_i((1-\beta)\widehat{w}_i + \beta w_k)), \quad (12)$$

where  $w_k$ s are random latent codes,  $G_i$  and  $D_i$  are the generator and the discriminator for the component  $C_i$  and  $\beta$  determines the extent of interpolation, controlling the localization of our loss. Our fine-tuning formulation thus becomes:

$$\arg \min_{\theta_{G_i}, i \in 1 \dots n} \mathcal{L}_G + \lambda_{LD} \mathcal{L}_{LD}, \quad (13)$$

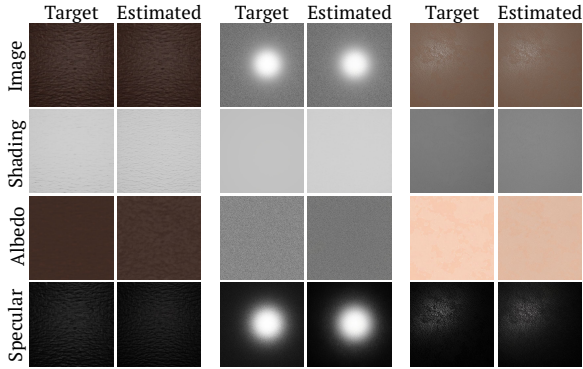


Figure 3. **Decomposition results for synthetic Materials.** Three examples are shown. Again, left column, from top to bottom, target Image (used for optimization), GT shading, and albedo. The right column contains our estimates. We are able to correctly separate the highlights and to discriminate between darker shading and darker albedo.

where  $\mathcal{L}_G$  is the generator loss as defined in Eq. 11. As discussed in the Ablation study (Sec. 5.4), the  $\mathcal{L}_{LD}$  loss helps maintaining the GAN priors during optimization even as multiple generators are fine-tuned together.

## 5. Experiments

In this section, we present a set of experiments that showcase the efficacy of our method. We provide intrinsic image decomposition results on two different datasets on both synthetic and real images along with comparisons with existing methods and ablation studies.

### 5.1. Preliminaries

For all our experiments we use StyleGAN2 [38] to train the generators and a pSp [64] encoder for initialization. All our generators and encoders are trained using their publicly available codebases and with the standard choices of the hyperparameters.

Our optimization-based inversion method remains the same for all the datasets with a learning rate of 0.1, kNN loss weight of 0.0001, and  $k = 50$ . We run the optimization for 1000 steps.

The decomposition results are evaluated using several metrics such as MSE, SSIM, LPIPS, and PSNR for the synthetic images that provide ground truth. We also provide comparisons with several state-of-the-art methods that are used in the literature for intrinsic image decomposition. The results demonstrate the effectiveness of our proposed method in decomposing the input images into their intrinsic components and the ability to handle real images.

### 5.2. Experiments on Materials data

The Materials dataset is composed of highly realistic renderings of synthetic material tiles as done in Deschaintre et

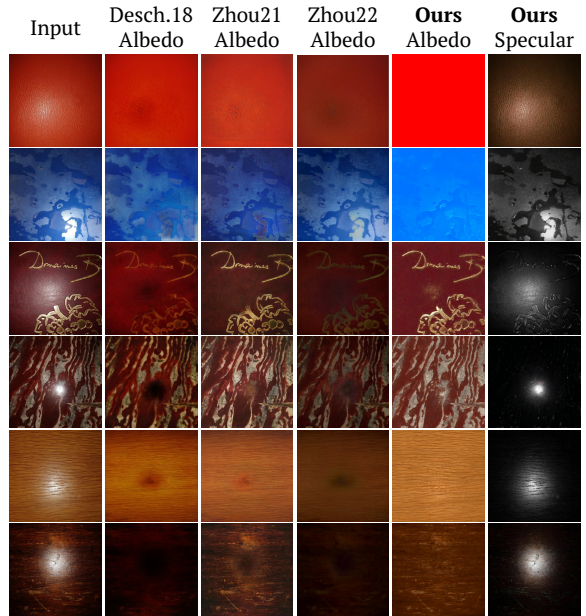


Figure 4. **Comparisons for Albedo estimation on real material pictures.** Our GAN priors allow us to better separate the highlight from the albedo leading to fewer visual artifacts. Our recovered specular layer is shown on the right for reference.

Table 1. **Quantitative comparisons on synthetic Materials.** We evaluate albedo estimation on 100 materials from our test dataset for our method and three recent SVBRDF estimation methods.

	Estimated Albedo		
	MSE↓	LPIPS↓	PSNR↑
Desch18 [19]	0.0211	0.314	19.53
Zhou21 [84]	0.0202	<b>0.293</b>	20.919
Zhou22 [85]	0.0213	0.296	20.18
Ours	<b>0.0146</b>	0.326	<b>21.58</b>

al. [19]. We obtain the albedo map directly from the material and compose the shading and specular components from blender direct and indirect rendering passes. More details on this dataset are given in the supplementary. For this dataset, we show results for decomposition into 3 components (albedo, shading, and specular; Eq. 6) and operate at the resolution of  $512 \times 512$ . For synthetic test images, we show results in Fig. 3 and quantitative comparisons to several recent SVBRDF estimation methods [19, 84, 85] on the task of albedo recovery in Tab. 1. While we do not recover the full SVBRDF as these methods do, we do show competitive results on albedo map recovery both quantitatively and qualitatively on real images, taken from Deschaintre et al. [20], visible in Fig. 4. As can be seen, our GAN priors allow to correctly separate flash highlights from the diffuse component and to recover plausible content under the highlights in the albedo map while correcting for the lighting fall-off. Additional results are provided in the supplementary (Fig. 16, 17).

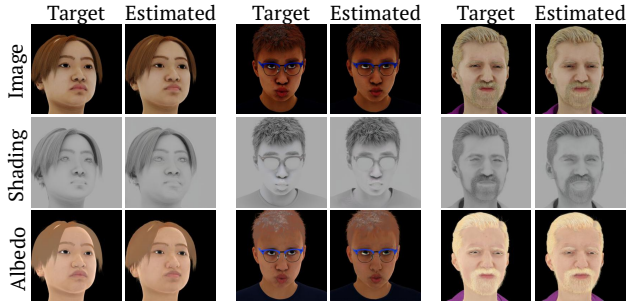


Figure 5. **Two components decomposition results for Lumos Faces dataset.** On synthetic data, our estimated components are close to the ground truth, generator tuning is not needed when testing data is close to the GAN training distribution.

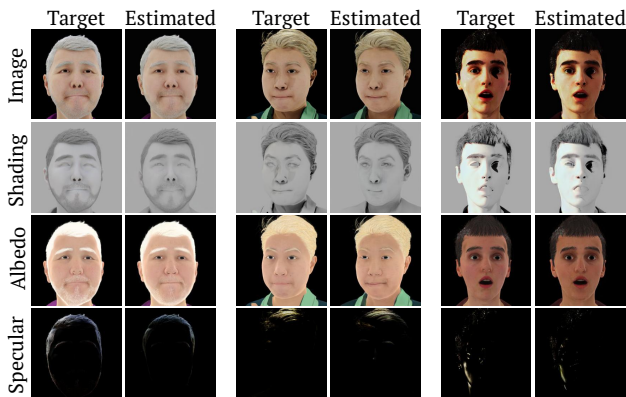


Figure 6. **Three components decomposition results for Lumos Faces dataset.** Using three components allows to recover subtle specular effects.

### 5.3. Experiments on Faces data

Faces are notoriously adapted to the usage of GANs and to cater to such a use case, we use the synthetic Lumos dataset [79] to train our GANs, we defer more discussions on the dataset to the supplementary.

First, we show results on test images from the dataset in Fig. 5 and Fig. 6 where we use respectively two and three components. For this experiment, we use the encoder initialization and our optimization without generator fine-tuning (PTI). As can be seen in these figures our method is able to recover accurate albedo, shading, and specular maps and does not suffer from cross-channel contamination.

As the synthetic dataset does not reproduce the complexity and diversity of real faces, for real images, we add the generator fine-tuning step presented in Sec. 4.2. We show results on real faces taken from the FFHQ dataset in Fig. 7 and compare our method to five recent relighting methods, Total Relighting [57], Lumos [79], InverseRenderNet++ [81], PieNet [18], and Nextface [21–23], that seek to recover face albedo as part of their relighting pipeline, this is shown in Fig. 9. In all the cases, the predicted com-

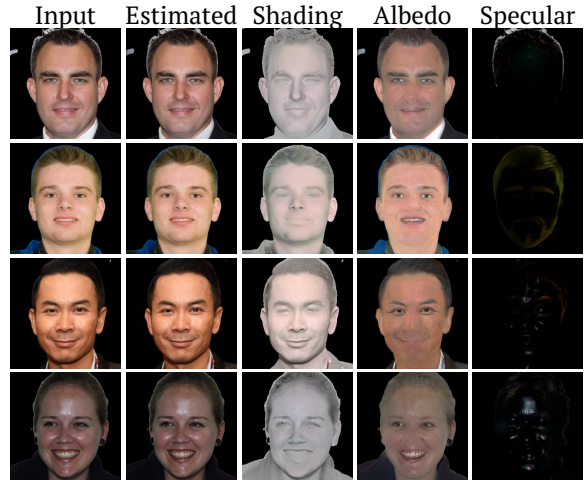


Figure 7. **Decomposition results for real faces.** Using generator fine-tuning our method generalizes to real faces and correctly separates albedo, shading, and specular effects while reconstructing the input correctly.



Figure 8. **Face relighting results.** Once the IID is obtained, we modify the shading component using GAN editing technique [68] on the shading generator obtaining plausible relighting edits.

ponents by our method maintain the priors of each GAN. In the comparison figure we can observe that our method works better at producing shading-free albedo images. Notably, our predicted albedo contains fewer shading variations around the neck, nose, nostrils, and mouth.

For quantitative comparisons, we use a test set of synthetic images from Lumos dataset, and compare reconstruction errors for albedo recovery for all variants of our approach with four competing methods in Tab. 3. We see that our method achieves the lowest errors. We provide additional results on both synthetic and real faces in the supplementary (Fig. 18, 19, 20, 21).

**Application to relighting.** GANs are known for the rich image manipulation capabilities they offer. We show real image relighting results in Fig. 8. To generate these results, after obtaining the inversions for albedo, shading, and specular, we use an off-the-shelf latent space editing method SeFa [68] on the shading generator to modify the shading image while keeping the other two components constant. StyleGAN’s disentangled representation helps with identity preservation. As seen in Fig. 8, our approach produces varied novel lighting.

Table 2. **Quantitative comparisons** between different variations of our approach on Lumos Faces synthetic dataset

	Faces											
	Albedo			Shading			Specular			Image		
	LPIPS↓	MSE↓	PSNR↑									
Inversion w/ single GAN for both albedo and shading	0.1954	0.1269	14.1662	0.2657	0.07021	18.2450	-	-	-	0.09342	0.03133	24.4665
Optimization	0.1311	0.0417	22.4763	0.2832	0.0518	18.8636	0.2544	0.0336	32.3207	0.0879	0.0308	24.2962
Opt. + InDomain loss	0.1209	0.0400	22.5891	0.2738	0.0497	19.1599	0.2444	0.0332	32.8339	0.0876	0.0302	24.1644
Opt. + kNN loss	0.1047	0.0357	23.5331	0.2603	0.0487	20.911	0.2361	0.0320	32.9050	0.0868	0.0301	24.1144
Encoder + Opt. + kNN loss	0.0887	0.0345	24.1467	0.2039	0.0414	21.0323	0.1722	0.0282	33.4090	0.0713	0.0306	26.4451
Encoder + Opt. + kNN loss + PTI w/o D Loss	0.0784	0.0155	24.1160	0.2775	0.0519	18.1651	0.1550	0.0278	32.8380	<b>0.0136</b>	<b>0.0011</b>	<b>33.5454</b>
Encoder + Opt. + kNN loss + PTI w/ D Loss	<b>0.0765</b>	<b>0.0072</b>	<b>27.3401</b>	<b>0.1703</b>	<b>0.0285</b>	<b>22.4754</b>	<b>0.0774</b>	<b>0.0251</b>	<b>34.5475</b>	0.0194	0.0022	32.5175

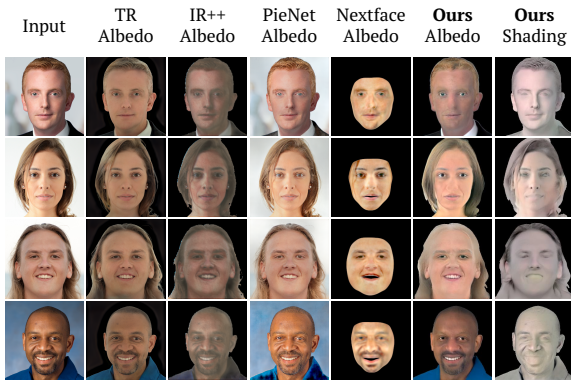


Figure 9. **Comparison of our method on real face images.** On real faces, our approach can recover more faithful albedo by removing shadows, and preserving the appropriate skin tones as compared to other competing methods.

Table 3. **Quantitative comparisons** on Synthetic Faces testset

On synthetic faces (Lumos dataset)	Estimated Albedo		
	LPIPS↓	MSE↓	PSNR↑
Total Relighting [57]	0.2220	0.0644	17.1470
PieNet [18]	0.1843	0.0501	19.4761
InverseRenderNet++ [81]	0.3794	0.1550	14.5227
NextFace [21–23]	0.2034	0.0791	19.0699
<b>Ours:</b>			
Optimization	0.1311	0.0417	22.4763
Opt. + kNN loss	0.1047	0.0357	23.5331
Encoder + Opt. + kNN loss	0.0887	0.0345	24.1467
Encoder + Opt. + kNN loss + PTI w/o D Loss	0.0784	0.0155	24.1160
Encoder + Opt. + kNN loss + PTI w/ D Loss	<b>0.0765</b>	<b>0.0072</b>	<b>27.3401</b>

#### 5.4. Ablation studies

In this section, we illustrate the benefits of each component of our method.

**Advantage of independently trained GANs.** Training GANs independently makes our pipeline modular and flexible: different components can be trained with different data sources, and new components can be easily introduced in the forward model without re-training the entire pipeline. We showcase such use case by adding the specular component to the albedo-shading forward model (Fig. 6, 7, 3, 4).

We also show that it is easier to train and invert GANs independently, further preventing cross-contamination during inversion. To demonstrate this, we train a single multi-component GAN that learns to generate both albedo and shading images simultaneously by producing a 6-channel output: 3 channels each for albedo and shading. We increase the number of trainable parameters by a factor of two to keep the capacity of the model comparable with our method.

First, as shown in Fig. 10, such joint training leads to inferior image generation compared to independently-trained albedo and shading GANs. With a single GAN, albedo and shading are leaking into each other, this is also measured by higher FID scores.

Second, having the same network generating both albedo and shading means that the information is entangled up to the last layer, leading to cross-contamination during inversion. This can be seen in Fig. 11. While the image reconstruction quality is equivalent, the inversion is better using multiple GANs. Our observation is also supported with the quantitative results provided in Tab. 2.

Table 4. **Effectiveness of kNN Loss in GAN Inversion**

On CelebA-HQ test set	Inversion on single GAN trained on FFHQ		
	LPIPS↓	MSE↓	PSNR↑
Optimization [38]	0.3841	0.0950	16.9077
Opt. + InDomain loss [71, 87]	0.3839	0.0941	16.9901
Opt. + kNN loss ( <b>Ours</b> )	<b>0.3789</b>	<b>0.0919</b>	<b>17.1202</b>

**Effectiveness of kNN loss.** We evaluate the effectiveness of our newly proposed kNN-loss. For a fair evaluation, we first provide experiments for the more general single GAN inversion setup: we use a StyleGAN2 model trained on natural face images from FFHQ dataset [35], and invert CelebA-HQ testset [34] images using optimization-based inversion [38]. As shown in Tab. 4, using kNN loss as a regularization during optimization improves the performance over direct optimization and optimization with In-Domain loss.

**Full method ablations.** Finally, we present a comprehensive set of ablations for our joint inversion of multiple

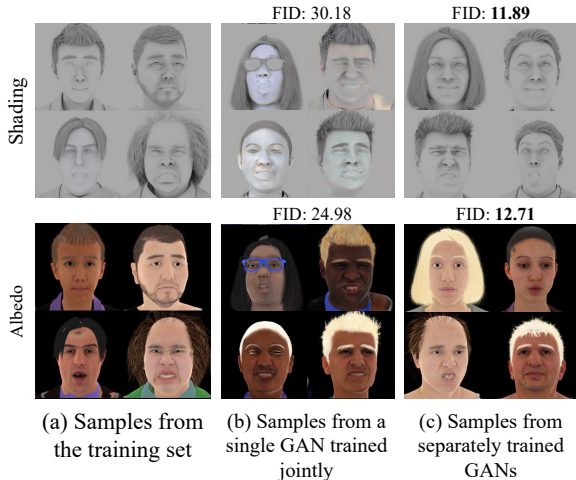


Figure 10. **Single vs Separated GANs.** Training separate GAN for each component results in better generation quality as opposed to training a single GAN for learning both components.

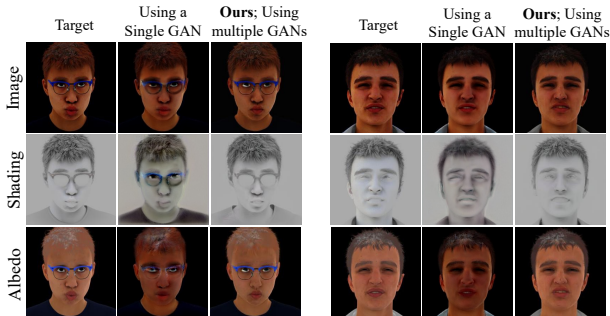


Figure 11. **Single vs Separated GANs Inversion.** Inversion on a single GAN trained to generate both albedo and shading leads to cross-contamination issues (note the color leakage in shading and shadow effects in albedo). We mitigate this issue by training independent GANs for each component.

GANs. We provide qualitative results (Fig. 12) and quantitative evaluations for intrinsic image decomposition on the Lumos Faces dataset in Tab. 2, second part.

We first evaluate our method using only direct Optimization (Opt.). We then add the InDomain Loss discussed in Sec. 3.4 and then replace it with our kNN loss. As can be seen in Tab. 2 the kNN Loss allows better recovery of the intrinsic components by maintaining the latent codes within domain, it also outperforms the in-domain loss.

We then add the encoder initialization from Sec. 4.1 to the pipeline and finally add the PTI-based finetuning, without, then with, the discriminator loss (D Loss) as discussed in Sec. 4.2. Our evaluation shows that the encoder initialization brings a clear improvement in both reconstruction quality and component estimations. The PTI without D Loss does improve the reconstruction of the input image but degrades the performance of component estimation, whereas, with the D Loss, the PTI still improves the image recon-

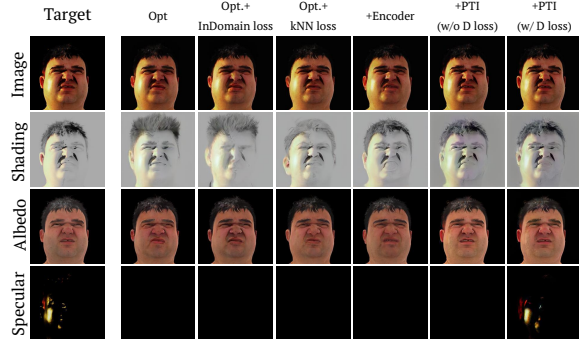


Figure 12. **Ablation study on Lumos synthetic face dataset.** Our decomposition improves as we (from left to right) replace In-Domain loss with kNN loss; initialize with and encoder; use PTI scheme to finetune generators; and use local D loss during the PTI fine-tuning step.

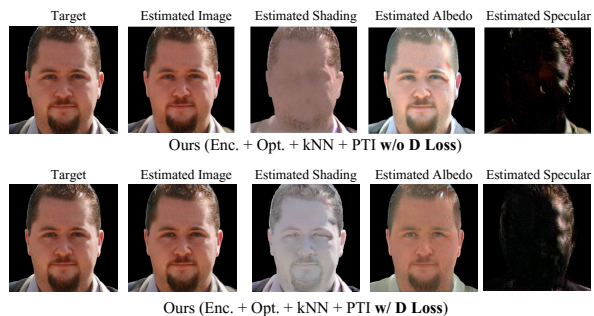


Figure 13. **Importance of local D loss.** Local D loss preserves the generator priors by preventing the local manifold from distortions. Above we show IID on a real face image without (top) and with (bottom) local discriminator loss.

struction quality but also provides the best results for the decomposition. A qualitative visualization of this difference is visible in Fig. 13.

## 6. Discussion and Future Work

In this paper, we introduced JoIN a new method to solve inverse imaging problems using a bank of GANs. We show it is possible to retain GANs distribution priors while jointly inverting several of them in the case of Intrinsic Image Decomposition. Nonetheless, our method inherits some drawbacks of GAN inversion methods. First, it is slower than feed-forward methods with runtimes of a few seconds. Second, currently, training GANs on unaligned distributions remains a complex task and our method can be limited by the GAN training quality, hence it is more adapted to distributions that GANs can model well such as face images. In the future, as new generative models emerge, we believe our method will be applicable to broader datasets and could be tested on a wider variety of problems, possibly extending the ideas beyond images.

## References

- [1] Rameen Abdal, Yipeng Qin, and Peter Wonka. Image2stylegan: How to embed images into the stylegan latent space? In *Proceedings of the IEEE/CVF International Conference on Computer Vision*, pages 4432–4441, 2019. 2
- [2] Rameen Abdal, Yipeng Qin, and Peter Wonka. Image2stylegan++: How to edit the embedded images? In *Proceedings of the IEEE/CVF conference on computer vision and pattern recognition*, pages 8296–8305, 2020. 2
- [3] Miika Aittala, Tim Weyrich, and Jaakko Lehtinen. Two-shot svbrdf capture for stationary materials. *ACM Trans. Graph.*, 34(4), 2015. 2
- [4] Yuval Alaluf, Or Patashnik, and Daniel Cohen-Or. Restyle: A residual-based stylegan encoder via iterative refinement. In *Proceedings of the IEEE/CVF International Conference on Computer Vision*, pages 6711–6720, 2021. 2
- [5] Jonathan T. Barron and Jitendra Malik. Shape, illumination, and reflectance from shading. *IEEE Trans. Pattern Anal. Mach. Intell.*, 37(8):1670–1687, 2015. 1
- [6] David Bau, Hendrik Strobel, William S. Peebles, Jonas Wulff, Bolei Zhou, Jun-Yan Zhu, and Antonio Torralba. Semantic photo manipulation with a generative image prior. *ACM Transactions on Graphics (TOG)*, 38:1–11, 2019. 2
- [7] David Bau, Jun-Yan Zhu, Jonas Wulff, William Peebles, Hendrik Strobel, Bolei Zhou, and Antonio Torralba. Seeing what a gan cannot generate. In *Proceedings of the IEEE/CVF International Conference on Computer Vision*, pages 4502–4511, 2019.
- [8] David Bau, Jun-Yan Zhu, Jonas Wulff, William S. Peebles, Hendrik Strobel, Bolei Zhou, and Antonio Torralba. Seeing what a gan cannot generate. *ICCV*, pages 4501–4510, 2019. 2, 4
- [9] Anand Bhattad, Daniel McKee, Derek Hoiem, and David Alexander Forsyth. Stylegan knows normal, depth, albedo, and more. *ArXiv*, abs/2306.00987, 2023. 2
- [10] Blender Online Community. *Blender - a 3D modelling and rendering package*. Blender Foundation, Blender Institute, Amsterdam, 2023. 12
- [11] Nicolas Bonneel, Kalyan Sunkavalli, James Tompkin, Deqing Sun, Sylvain Paris, and Hanspeter Pfister. Interactive intrinsic video editing. *ACM Transactions on Graphics (Proceedings of SIGGRAPH Asia 2014)*, 33(6), 2014. 2
- [12] Ashish Bora, Ajil Jalal, Eric Price, and Alexandros G. Dimakis. Compressed sensing using generative models. In *International Conference on Machine Learning*, 2017. 1
- [13] Adrien Bousseau, Sylvain Paris, and Frédo Durand. User Assisted Intrinsic Images. *ACM Transactions on Graphics*, 28(5):130:1–10, 2009. 1, 2
- [14] Andrew Brock, Theodore Lim, James M Ritchie, and Nick Weston. Neural photo editing with introspective adversarial networks. *arXiv preprint arXiv:1609.07093*, 2016. 2
- [15] Lucy Chai, Jonas Wulff, and Phillip Isola. Using latent space regression to analyze and leverage compositionality in gans. *ICLR*, 2021. 2
- [16] Lucy Chai, Jun-Yan Zhu, Eli Shechtman, Phillip Isola, and Richard Zhang. Ensembling with deep generative views. In *CVPR*, 2021. 2, 4
- [17] Antonia Creswell and Anil Anthony Bharath. Inverting the generator of a generative adversarial network. *IEEE Transactions on Neural Networks and Learning Systems*, 30:1967–1974, 2019. 2
- [18] Partha Das, Sezer Karaoglu, Arjan Gisenij, and Theo Gevers. Signet: Intrinsic image decomposition by a semantic and invariant gradient driven network for indoor scenes. In *European Conference of Computer Vision Workshop CV4Metaverse 2022 (ECCV)*, 2022. 6, 7
- [19] Valentin Deschaintre, Miika Aittala, Fredo Durand, George Drettakis, and Adrien Bousseau. Single-image svbrdf capture with a rendering-aware deep network. *ACM Trans. Graph.*, 37(4), 2018. 2, 5
- [20] Valentin Deschaintre, Miika Aittala, Fredo Durand, George Drettakis, and Adrien Bousseau. Flexible svbrdf capture with a multi-image deep network. *Computer Graphics Forum*, 38(4):1–13, 2019. 2, 5
- [21] Abdallah Dib, Gaurav Bharaj, Junghyun Ahn, Cédric Thébault, Philippe Gosselin, Marco Romeo, and Louis Chevallier. Practical face reconstruction via differentiable ray tracing. In *Computer Graphics Forum*, pages 153–164. Wiley Online Library, 2021. 6, 7
- [22] Abdallah Dib, Cedric Thebault, Junghyun Ahn, Philippe-Henri Gosselin, Christian Theobalt, and Louis Chevallier. Towards high fidelity monocular face reconstruction with rich reflectance using self-supervised learning and ray tracing. In *Proceedings of the IEEE/CVF International Conference on Computer Vision*, pages 12819–12829, 2021.
- [23] Abdallah Dib, Junghyun Ahn, Cedric Thebault, Philippe-Henri Gosselin, and Louis Chevallier. S2f2: Self-supervised high fidelity face reconstruction from monocular image. *arXiv preprint arXiv:2203.07732*, 2022. 6, 7
- [24] Sylvain Duchêne, Clement Riant, Gaurav Chaurasia, Jorge Lopez-Moreno, Pierre-Yves Laffont, Stefan Popov, Adrien Bousseau, and George Drettakis. Multi-view intrinsic images of outdoors scenes with an application to relighting. *ACM Transactions on Graphics (TOG)*, 34(5), 2015. 2
- [25] Qianli Feng, Viraj Shah, Raghudeep Gadde, Pietro Perona, and Aleix Martinez. Near perfect gan inversion. *ArXiv*, abs/2202.11833, 2022. 2, 4
- [26] David Griffiths, Tobias Ritschel, and Julien Philip. Outcast: Single image relighting with cast shadows. *Computer Graphics Forum*, 43, 2022. 2
- [27] Jinjin Gu, Yujun Shen, and Bolei Zhou. Image processing using multi-code gan prior. *2020 IEEE/CVF Conference on Computer Vision and Pattern Recognition (CVPR)*, pages 3009–3018, 2019. 1
- [28] Yu Guo, Cameron Smith, Miloš Hašan, Kalyan Sunkavalli, and Shuang Zhao. Materialgan: Reflectance capture using a generative svbrdf model. *ACM Trans. Graph.*, 39(6), 2020. 1, 2
- [29] Paul Hand, Oscar Leong, and Vladislav Voroninski. Phase retrieval under a generative prior. *ArXiv*, abs/1807.04261, 2018. 1
- [30] Berthold K.P. Horn. Determining lightness from an image. *Computer Graphics and Image Processing*, 3(4):277–299, 1974. 2

- [31] Andrew Hou, Ze Zhang, Michel Sarkis, Ning Bi, Yiyang Tong, and Xiaoming Liu. Towards high fidelity face relighting with realistic shadows. In *Proceedings of the IEEE/CVF Conference on Computer Vision and Pattern Recognition (CVPR)*, pages 14719–14728, 2021. 2
- [32] Minyoung Huh, Richard Zhang, Jun-Yan Zhu, Sylvain Paris, and Aaron Hertzmann. Transforming and projecting images into class-conditional generative networks. In *European Conference on Computer Vision*, pages 17–34. Springer, 2020. 2
- [33] Rakib Hyder, Viraj Shah, Chinmay Hegde, and M. Salman Asif. Alternating phase projected gradient descent with generative priors for solving compressive phase retrieval. *ICASSP 2019 - 2019 IEEE International Conference on Acoustics, Speech and Signal Processing (ICASSP)*, pages 7705–7709, 2019. 1
- [34] Tero Karras, Timo Aila, Samuli Laine, and Jaakko Lehtinen. Progressive growing of gans for improved quality, stability, and variation. In *International Conference on Learning Representations*, 2018. 7, 13
- [35] Tero Karras, Samuli Laine, and Timo Aila. A style-based generator architecture for generative adversarial networks. In *Proceedings of the IEEE conference on computer vision and pattern recognition*, pages 4401–4410, 2019. 7, 13
- [36] Tero Karras, Samuli Laine, and Timo Aila. A style-based generator architecture for generative adversarial networks, 2019. 3
- [37] Tero Karras, Samuli Laine, Miika Aittala, Janne Hellsten, Jaakko Lehtinen, and Timo Aila. Analyzing and improving the image quality of StyleGAN. In *Proc. CVPR*, 2020. 3
- [38] Tero Karras, Samuli Laine, Miika Aittala, Janne Hellsten, Jaakko Lehtinen, and Timo Aila. Analyzing and improving the image quality of stylegan. In *Proceedings of the IEEE/CVF Conference on Computer Vision and Pattern Recognition*, pages 8110–8119, 2020. 2, 3, 5, 7
- [39] Markus Kettunen, Erik Härkönen, and Jaakko Lehtinen. Ellips: Robust perceptual image similarity via random transformation ensembles. *ArXiv*, abs/1906.03973, 2019. 3
- [40] Pierre-Yves Laffont, Adrien Bousseau, Sylvain Paris, Frédo Durand, and George Drettakis. Coherent intrinsic images from photo collections. *ACM Transactions on Graphics (TOG)*, 31(6), 2012. 2
- [41] Pierre-Yves Laffont, Adrien Bousseau, and George Drettakis. Rich intrinsic image decomposition of outdoor scenes from multiple views. *IEEE Transactions on Visualization and Computer Graphics*, 19(2):210 – 224, 2013. presented at SIGGRAPH 2012 (Talk and Poster sessions). 2
- [42] Edwin H. Land and John J. McCann. Lightness and retinex theory. *J. Opt. Soc. Am.*, 61(1):1–11, 1971. 2
- [43] Anders Boesen Lindbo Larsen, Søren Kaae Sønderby, H. Larochelle, and Ole Winther. Autoencoding beyond pixels using a learned similarity metric. *ArXiv*, abs/1512.09300, 2016. 2
- [44] Christian Ledig, Lucas Theis, Ferenc Huszár, Jose Caballero, Andrew P. Aitken, Alykhan Tejani, Johannes Totz, Zehan Wang, and Wenzhe Shi. Photo-realistic single image super-resolution using a generative adversarial network. *2017 IEEE Conference on Computer Vision and Pattern Recognition (CVPR)*, pages 105–114, 2016. 1
- [45] Zhengqi Li and Noah Snavely. Learning intrinsic image decomposition from watching the world. In *Computer Vision and Pattern Recognition (CVPR)*, 2018. 2
- [46] Zhengqi Li and Noah Snavely. Cgintrinsics: Better intrinsic image decomposition through physically-based rendering. In *Proceedings of the European Conference on Computer Vision (ECCV)*, pages 371–387, 2018.
- [47] Zhengqin Li, Mohammad Shafiei, Ravi Ramamoorthi, Kalyan Sunkavalli, and Manmohan Chandraker. Inverse rendering for complex indoor scenes: Shape, spatially-varying lighting and svbrdf from a single image. In *Proceedings of the IEEE/CVF Conference on Computer Vision and Pattern Recognition*, pages 2475–2484, 2020. 1, 2
- [48] Zachary Chase Lipton and Subarna Tripathi. Precise recovery of latent vectors from generative adversarial networks. *ArXiv*, abs/1702.04782, 2017. 2
- [49] Zachary C Lipton and Subarna Tripathi. Precise recovery of latent vectors from generative adversarial networks. In *International Conference on Learning Representations Workshops*, 2017. 2
- [50] Yunfei Liu, Yu Li, Shaodi You, and Feng Lu. Unsupervised learning for intrinsic image decomposition from a single image. In *Proceedings of the IEEE/CVF Conference on Computer Vision and Pattern Recognition (CVPR)*, 2020. 2
- [51] Xudong Mao, Liujuan Cao, Aurele Tohokantche Gnanha, Zhenguang Yang, Qing Li, and Rongrong Ji. Cycle encoding of a stylegan encoder for improved reconstruction and editability. *Proceedings of the 30th ACM International Conference on Multimedia*, 2022. 2
- [52] Abhimitra Meka, Michael Zollhofer, Christian Richardt, and Christian Theobalt. Live intrinsic video. *ACM Transactions on Graphics (Proceedings SIGGRAPH)*, 35(4), 2016. 2
- [53] Abhimitra Meka, Mohammad Shafiei, Michael Zollhofer, Christian Richardt, and Christian Theobalt. Real-time global illumination decomposition of videos. In *ACM Transactions on Graphics*, 2021. 2
- [54] Seung Jun Moon and GyeongMoon Park. Interestyle: Encoding an interest region for robust stylegan inversion. In *ECCV*, 2022. 2
- [55] Thomas Nestmeyer and Peter V Gehler. Reflectance adaptive filtering improves intrinsic image estimation. In *Computer Vision and Pattern Recognition (CVPR)*, 2017. 2
- [56] Yuzhen Niu, Jianbin Wu, Wenxi Liu, Wenzhong Guo, and Rynson W. H. Lau. Hdr-gan: Hdr image reconstruction from multi-exposed ldr images with large motions. *IEEE Transactions on Image Processing*, 30:3885–3896, 2020. 1
- [57] Rohit Pandey, Sergio Orts Escolano, Chloe LeGendre, Christian Haene, Sofien Bouaziz, Christoph Rhemann, Paul Debevec, and Sean Fanello. Total relighting: Learning to relight portraits for background replacement. In *ACM Transactions on Graphics (Proceedings SIGGRAPH)*, 2021. 2, 6, 7
- [58] Guim Perarnau, Joost Van De Weijer, Bogdan Raducanu, and Jose M Álvarez. Invertible conditional gans for image editing. *arXiv preprint arXiv:1611.06355*, 2016. 2

- [59] Julien Philip, Michaël Gharbi, Tinghui Zhou, Alexei Efros, and George Drettakis. Multi-view relighting using a geometry-aware network. *ACM Transactions on Graphics*, 2019. [2](#)
- [60] Julien Philip, Sébastien Morgenthaler, Michaël Gharbi, and George Drettakis. Free-viewpoint indoor neural relighting from multi-view stereo. *ACM Transactions on Graphics*, 2021. [2](#)
- [61] Stanislav Pidhorskyi, Donald A Adjeroh, and Gianfranco Doretto. Adversarial latent autoencoders. In *Proceedings of the IEEE/CVF Conference on Computer Vision and Pattern Recognition*, pages 14104–14113, 2020. [2](#)
- [62] Erik Reinhard, Michael Stark, Peter Shirley, and James Ferwerda. Photographic tone reproduction for digital images. *ACM Transactions on Graphics*, 21, 2002. [12](#), [13](#)
- [63] Elad Richardson, Yuval Alaluf, Or Patashnik, Yotam Nitzan, Yaniv Azar, Stav Shapiro, and Daniel Cohen-Or. Encoding in style: a stylegan encoder for image-to-image translation. *CVPR*, 2021. [2](#), [4](#)
- [64] Elad Richardson, Yuval Alaluf, Or Patashnik, Yotam Nitzan, Yaniv Azar, Stav Shapiro, and Daniel Cohen-Or. Encoding in style: a stylegan encoder for image-to-image translation. In *Proceedings of the IEEE/CVF conference on computer vision and pattern recognition*, pages 2287–2296, 2021. [5](#)
- [65] Daniel Roich, Ron Mokady, Amit H. Bermano, and Daniel Cohen-Or. Pivotal tuning for latent-based editing of real images. *ACM Transactions on Graphics (TOG)*, 2021. [2](#), [4](#)
- [66] Viraj Shah and Chinmay Hegde. Solving linear inverse problems using gan priors: An algorithm with provable guarantees. *2018 IEEE International Conference on Acoustics, Speech and Signal Processing (ICASSP)*, pages 4609–4613, 2018. [1](#)
- [67] Viraj Shah and Chinmay Hegde. Solving linear inverse problems using gan priors: An algorithm with provable guarantees. In *2018 IEEE international conference on acoustics, speech and signal processing (ICASSP)*, pages 4609–4613. IEEE, 2018. [2](#)
- [68] Yujun Shen and Bolei Zhou. Closed-form factorization of latent semantics in gans. In *CVPR*, 2021. [6](#), [14](#), [15](#)
- [69] M.F. Tappen, W.T. Freeman, and E.H. Adelson. Recovering intrinsic images from a single image. *IEEE Transactions on Pattern Analysis and Machine Intelligence*, 27(9):1459–1472, 2005. [1](#)
- [70] Marshall F Tappen, William T Freeman, and Edward H Adelson. Recovering intrinsic images from a single image. In *Advances in neural information processing systems*, pages 1367–1374, 2003. [2](#)
- [71] Omer Tov, Yuval Alaluf, Yotam Nitzan, Or Patashnik, and Daniel Cohen-Or. Designing an encoder for stylegan image manipulation. *ACM Transactions on Graphics (TOG)*, 40(4): 1–14, 2021. [2](#), [3](#), [7](#)
- [72] Tengfei Wang, Yong Zhang, Yanbo Fan, Jue Wang, and Qifeng Chen. High-fidelity gan inversion for image attribute editing. *arxiv:2109.06590*, 2021.
- [73] Tianyi Wei, Dongdong Chen, Wenbo Zhou, Jing Liao, Weiming Zhang, Lu Yuan, Gang Hua, and Nenghai Yu. A simple baseline for stylegan inversion. *arXiv preprint arXiv:2104.07661*, 2021. [2](#), [4](#)
- [74] Y. Weiss. Deriving intrinsic images from image sequences. In *Proceedings Eighth IEEE International Conference on Computer Vision. ICCV 2001*, pages 68–75 vol.2, 2001. [2](#)
- [75] Weihao Xia, Yulun Zhang, Yujiu Yang, Jing-Hao Xue, Bolei Zhou, and Ming-Hsuan Yang. Gan inversion: A survey. *arXiv preprint arXiv:2101.05278*, 2021. [2](#)
- [76] Xu Yao, Alasdair Newson, Yann Gousseau, and Pierre Hellier. A style-based gan encoder for high fidelity reconstruction of images and videos. *European conference on computer vision*, 2022. [2](#)
- [77] Genzhi Ye, Elena Garces, Yebin Liu, Qionghai Dai, and Diego Gutierrez. Intrinsic video and applications. *ACM Transactions on Graphics (SIGGRAPH 2014)*, 33(4), 2014. [2](#)
- [78] Raymond A. Yeh, Chen Chen, Teck-Yian Lim, Alexander G. Schwing, Mark A. Hasegawa-Johnson, and Minh N. Do. Semantic image inpainting with deep generative models. *2017 IEEE Conference on Computer Vision and Pattern Recognition (CVPR)*, pages 6882–6890, 2016. [1](#)
- [79] Yu-Ying Yeh, Koki Nagano, Sameh Khamis, Jan Kautz, Ming-Yu Liu, and Ting-Chun Wang. Learning to relight portrait images via a virtual light stage and synthetic-to-real adaptation. *ACM Transactions on Graphics (TOG)*, 2022. [2](#), [6](#), [13](#)
- [80] Ye Yu and William AP Smith. Inverserendernet: Learning single image inverse rendering. In *Proceedings of the IEEE/CVF Conference on Computer Vision and Pattern Recognition (CVPR)*, 2019. [2](#)
- [81] Ye Yu and William A. P. Smith. Outdoor inverse rendering from a single image using multiview self-supervision. *IEEE Transactions on Pattern Analysis and Machine Intelligence*, 2021. to appear. [6](#), [7](#)
- [82] Richard Zhang, Phillip Isola, Alexei A Efros, Eli Shechtman, and Oliver Wang. The unreasonable effectiveness of deep features as a perceptual metric. In *CVPR*, 2018. [3](#)
- [83] Tinghui Zhou, Philipp Krahenbuhl, and Alexei A. Efros. Learning data-driven reflectance priors for intrinsic image decomposition. In *Proceedings of the IEEE International Conference on Computer Vision (ICCV)*, 2015. [2](#)
- [84] Xilong Zhou and Nima Khademi Kalantari. Adversarial single-image svbrdf estimation with hybrid training. *Computer Graphics Forum*, 2021. [2](#), [5](#)
- [85] Xilong Zhou and Nima Khademi Kalantari. Look-ahead training with learned reflectance loss for single-image svbrdf estimation. *ACM Transactions on Graphics*, 41(6), 2022. [2](#), [5](#)
- [86] J. Zhu, P. Krähenbühl, E. Shechtman, and A. Efros. Generative visual manipulation on the natural image manifold. In *ECCV*, 2016. [2](#)
- [87] Jiapeng Zhu, Yujun Shen, Deli Zhao, and Bolei Zhou. In-domain gan inversion for real image editing. In *European conference on computer vision*, pages 592–608. Springer, 2020. [3](#), [7](#)

## Supplementary Material

We provide following as supplementary material to support the discussion and results of the main paper:

- In section 7, we discuss the intrinsic image decomposition experiments on primeshapes dataset. We come up with such fully synthetic dataset of simple shapes with variations of lights and materials in order to demonstrate the efficacy of our method with the two-component model (albedo and shading).
- In Sec. 8, we discuss our pipeline for generating and processing our datasets. Specifically, we discuss how we generate Primeshapes and Materials synthetic datasets using blender in python, and pre-processing steps involved for Lumos synthetic face dataset.
- In Sec. 10 we provide additional results for experiments discussed in the main paper to present supporting evidence for the claims made. In particular, we provide additional qualitative results for synthetic and real materials (Fig. 16, 17) and qualitative results for synthetic and real faces (Fig. 18, 19, 21). Additional qualitative comparisons with competing methods on real faces are provided in Fig. 20. We also provide additional results for image relighting on faces using our method in Fig. 22.

## 7. Experiments on Primeshapes data

We start with the simpler case of decomposing images for the Primeshapes dataset a fully synthetic dataset that contains rendered images of a variety of primitive shape objects under varying lighting conditions. We use this dataset to demonstrate the efficacy of our method with the two-component model (albedo and shading). We produce our decomposition using only optimization. We initialize the latent codes  $w_i$ s with the mean latent code  $\bar{w}_i$  of each GAN and apply the kNN loss in order to keep the  $w$ -code estimates in domain. As can be seen in Fig. 14, our method is able to achieve successful decomposition for this dataset re-

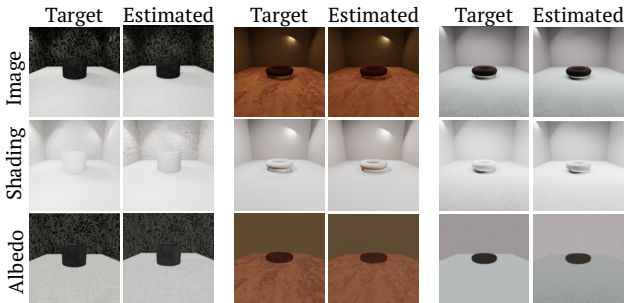


Figure 14. **Decomposition results for Primeshapes dataset.** Three examples are shown. For each, we show on the left column, from top to bottom, the target Image used for optimization, ground truth shading, and albedo for reference. The right column contains our estimates.

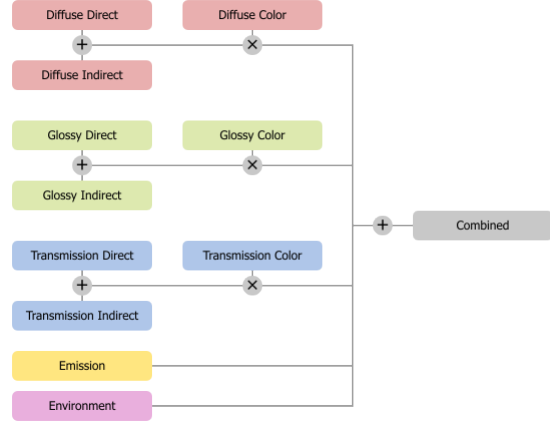


Figure 15. **Components available in our dataset.** (Image source: Blender documentation [10]).

taining each GANs priors and without cross-contamination. Note that while we show the target albedo and shading for each example, only the target image is used during optimization.

$$\text{final image} = \text{shading} \cdot \text{albedo} + \text{specular} \quad (14)$$

**Tone-mapping.** Since the renderings generated using blender are in linear space, we apply suitable tone-mapping to each of the image components in order to use them in the GAN/encoder training. Our choice of tone-mapping functions is standard, and the same for both Primeshapes and Materials datasets. For albedo, we use gamma/sRGB tone-mapping with  $\gamma = 2.4$ , while for shading and specular, we use Reinhard global tone-mapping [62] as these signals are inherently high-dynamic range.

## 8. Rendered Datasets details

**Data preparation pipeline.** We use the blender python package [10] to generate both the Primeshapes and Materials synthetic datasets. We make use of rendering and passes functionalities in blender python to render 11 components for each scene. Fig. 15 shows the relationship between these 11 components, and how they can be combined to obtain the image. We keep the pre-processing steps the same for both the Primeshapes and Materials datasets: we use the diffuse color component as albedo; we add diffuse direct and diffuse indirect to obtain shading; and for specular, we multiply glossy color with the sum of glossy direct and glossy indirect. We ignore the transmission, emission, and environment components in our inversion as they do not contribute significantly to the final image in our setting. Thus our composed image, used as the target for inversion, is obtained with:

## 8.1. Primeshapes Details

The Primeshapes dataset is a fully synthetic dataset containing rendered images of a variety of primitive shapes such as spheres, cones, cubes, cylinders, and toroids placed in a room with textured walls and lit by spotlights. Random materials chosen from a large collection of materials are assigned to the objects and the walls. The location of the lights is selected at random while the camera angle is kept fixed for all the images allowing easier training of GANs. This dataset contains 100,000 rendered images at the resolution of  $256 \times 256$ , out of which 70,000 images are used to train the StyleGAN generators and pSp encoders for individual components by using diffuse color as albedo, and the sum of direct and indirect shading as shading. The remaining 30,000 images are used as unseen testing images. To keep the problem simple in the context of the Primeshapes dataset, the inversion is run on a target image that does not use the glossy layers, thus using only the two components we aim at recovering (albedo and shading).

## 8.2. Materials Details

The Materials dataset is a fully synthetic dataset containing 80,000 renderings of materials taken from the Substance 3D collection. These synthetic materials are rendered with simulated flash lighting. Out of the full dataset, 1,000 images are left out to serve as a test set. To generate each sample, we randomly pick a distance to the material, an orientation of the surface, and a random light position close to the camera to simulate camera-light misalignment. We use a sphere light source with varying diameters and intensities. Images are rendered at  $512 \times 512$ .

## 9. Faces Dataset

The Lumos dataset [79] provides thousands of synthetic face images captured in virtual lightroom created inside a 3D design software. For each image, various intrinsic sub-components such as albedo, shadow, sub-surface scattering, specular etc. are also provided. We combine these sub-components to obtain albedo, shading, and specular maps used to train our GANs. We leverage the facial image alignment method used for the FFHQ dataset [34, 35] to pre-process each image in the Lumos dataset. Such pre-processing ensures that all the facial images are aligned in the same fashion, thus improving GAN training and allowing us to test our method on the real images from FFHQ.

**Data preparation pipeline for faces.** The Lumos synthetic dataset provides several image components for each face such as shadow, sub-surface scattering, coat, and sheen. While we use the albedo component directly from the dataset, we use the following strategy to obtain the shading and specular components for each image and train our

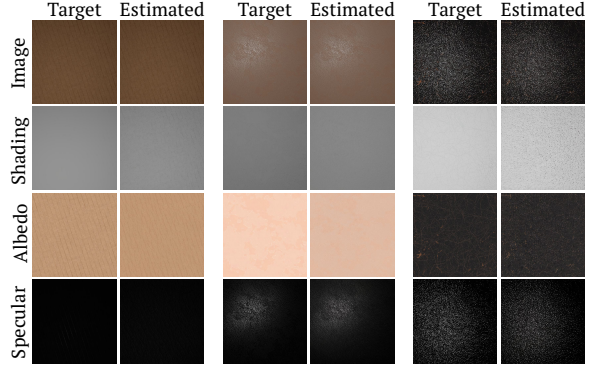


Figure 16. **Additional decomposition results for synthetic Materials.** Three examples are shown. Left column, from top to bottom, target Image (used for optimization), GT shading, and albedo. The right column contains our estimates. We are able to correctly separate the highlights and to discriminate between darker shading and darker albedo.

GANs:

$$\text{shading} = \text{shadow} + \frac{(\text{sub-surface scattering})}{\text{albedo}} \quad (15)$$

$$\text{specular} = \text{specular} + \text{sheen} + \text{coat} \quad (16)$$

We continue to use the Eq. 14 for faces as well in order to combine albedo, shading, and specular to get the final image. Our tone-mapping functions for the Lumos dataset are similar to the Materials dataset: for albedo we use gamma/sRGB tone-mapping with  $\gamma = 2.4$ , while for shading and specular, we use Reinhard tone-mapping [62].

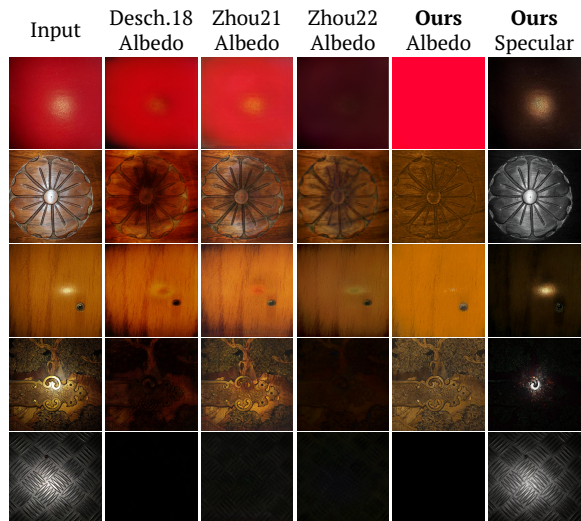


Figure 17. **Additional comparisons for Albedo estimation on real material pictures.** Our GAN priors allow us to better separate the highlight from the albedo leading to fewer visual artifacts. Our recovered specular layer is shown on the right for reference.

## 10. Additional Results.

We provide additional results and comparisons to support our claims, discussed in the main paper.

**Qualitative Results on Materials.** We provide additional results for decomposition on synthetic materials images in Fig. 16. As seen in the main paper, our model is able to recover albedo, shading, and specular components faithfully on synthetic images from Materials dataset. Further, we also provide additional comparisons with existing approaches on real material images in Fig. 17. Results are consistent with the qualitative and quantitative evaluations provided in the main manuscript.

**Qualitative Results on Faces.** We provide additional results for decomposition into 2 and 3 components on synthetic face images in Fig. 18 and Fig. 19 respectively. As seen in the main paper, our model is able to recover albedo, shading, and specular components faithfully on synthetic images from the Lumos dataset. Further, we also provide additional comparisons with other methods in Fig. 20, along with the results on the real images from the FFHQ dataset in Fig. 21. As discussed in the main paper, our method is able to preserve the GAN priors and separate the image into plausible components, without copying shading into the albedo image.

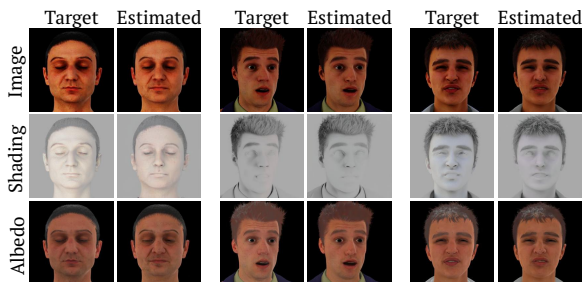


Figure 18. **Additional results for two components decomposition for Lumos Faces dataset.** On synthetic data, our component estimations are close to the ground truth, generator tuning is not needed when testing data is close to GAN training distribution.

**Image Relighting on Faces.** As discussed in the main paper, our modular approach allows leveraging latent space editing capabilities of GANs to modify each image component separately, making it suitable for image modification such as relighting applications. We show additional image relighting results on real faces in Fig. 22. After obtaining the inversions for albedo, shading, and specular, we use an off-the-shelf latent space editing method SeFa [68] on the shading generator to modify the shading image while keeping other components constant. StyleGAN’s disentangled representation allows the identity of the person to remain relatively constant as we modify the shading image. As seen in Fig. 22, our approach can produce varied novel lighting.

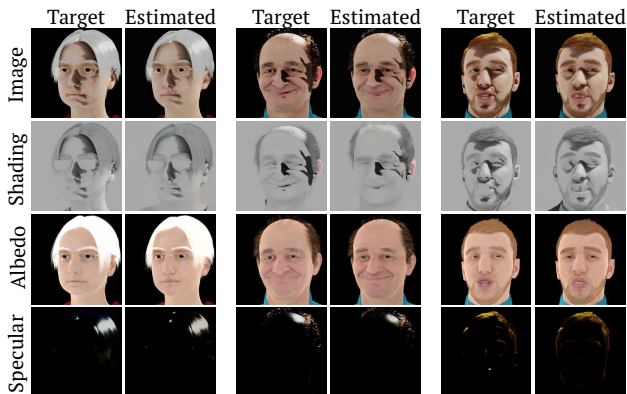


Figure 19. **Additional results for three components decomposition for Lumos Faces dataset.** Using three components allows to recover subtle specular effects.

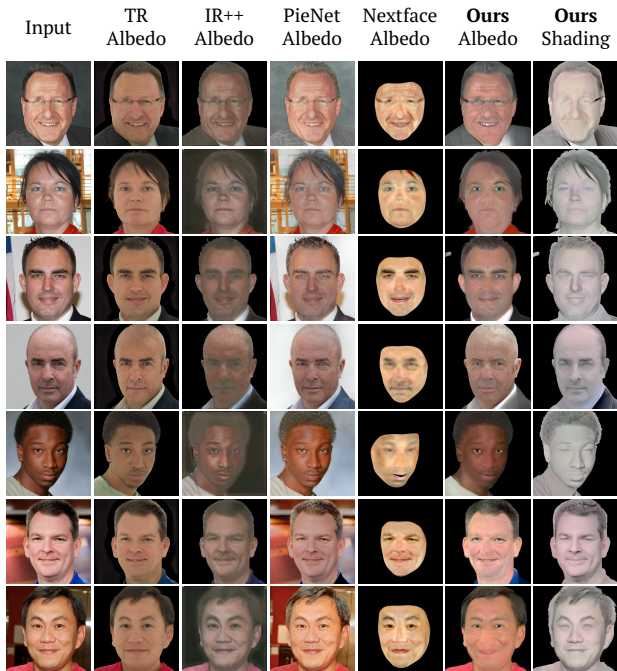


Figure 20. **Additional comparisons of our method on real face images.** On real faces, our approach can recover more faithful albedo by removing shadows, and preserving the appropriate skin tones as compared to other competing methods.

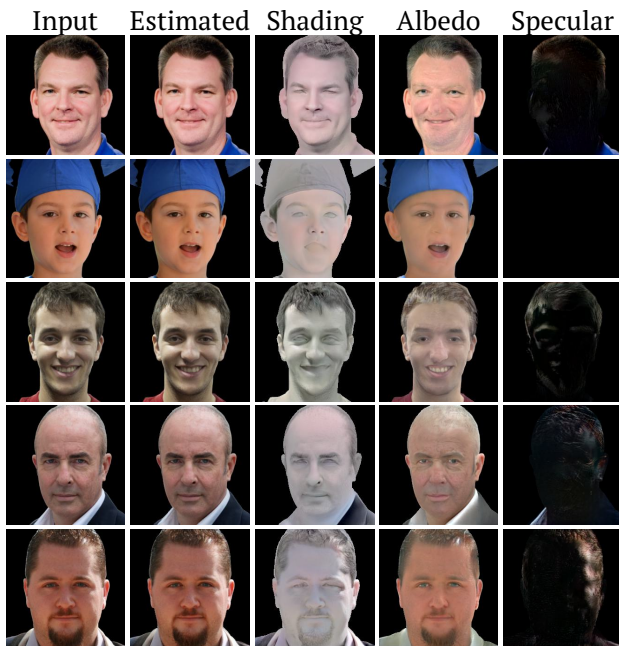


Figure 21. **Additional decomposition results for real faces.** Using generator fine-tuning our method generalizes to real faces and correctly separates albedo, shading, and specular effects while reconstructing the input correctly.

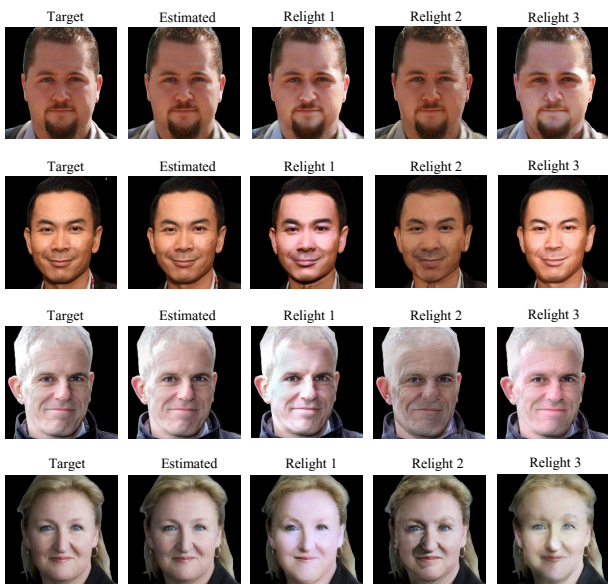


Figure 22. **Additional Face relighting results.** Once the IID is obtained, we modify the shading component using GAN editing technique [68] on the shading generator obtaining plausible relighting edits.